

SEISMIC INTERACTION AT SEPARATION JOINTS OF AN INSTRUMENTED CONCRETE BRIDGE

PRAVEEN K. MALHOTRA, MOH J. HUANG AND ANTHONY F. SHAKAL

California Strong Motion Instrumentation Program, Division of Mines and Geology, California Department of Conservation, 801 K Street, MS 13-35, Sacramento, CA 95814-3531, U.S.A.

SUMMARY

A multi-span, curved, concrete box-girder bridge has been extensively instrumented by the California Strong Motion Instrumentation Program (CSMIP) in cooperation with the California Department of Transportation (Caltrans). On 28 June 1992, the bridge was shaken by the magnitude 7.5 Landers and magnitude 6.6 Big Bear earthquakes in southern California. The epicentres of these earthquakes were 50 and 29 miles (81 and 46 km) from the bridge, respectively. All 34 strong-motion sensors installed on the bridge recorded the response to these earthquakes and provided an insightful set of data. A striking aspect of the response is the presence of intermittent sharp spikes in nearly all of the acceleration records from sensors at the deck of the bridge. Among these the highest spike was 0.8g for the Landers and 1.0g for the Big Bear earthquake. The peak ground acceleration at the bridge site was only about 0.1g for both these earthquakes. With the aid of visual examination and simple analysis it is deduced that (1) the spikes were caused by forces generated at separation joints by impacts and stretching of the cable restrainers between adjacent bridge segments; (2) the forces of impacts and cable stretching are directly proportional to the size of the spikes and can be estimated by the use of a simple formula; and (3) the spikes travelled from their source to other locations on the bridge with the velocity of a compression wave propagating through concrete.

INTRODUCTION

The California Strong Motion Instrumentation Program (CSMIP) of the Division of Mines and Geology in the Department of Conservation is installing strong-motion sensors on different structures and ground sites in California. The bridge structure examined here is one of the more than 100 stations from which strong-motion records were obtained during the 28 June, 1992 Landers and Big Bear earthquakes in California.

Bridge structure

The instrumented bridge (shown in Figure 1) is a multi-span, concrete structure that connects highways I-10 and I-215 in southern California, approximately 53 miles (85 km) from downtown Los Angeles. The bridge is curved in plan with radii of 1200 and 1300 ft (365 and 396 m), and has a total length of 2540 ft (774 m). The superstructure consists of a 41 ft (12.5 m) wide, 4-cell concrete box-girder that carries two lanes of traffic from eastbound I-10 to northbound I-215. There are five separation joints (hinges) in the box-girder that divide the bridge into six structures of different lengths and number of spans. The hinges are numbered 3, 7, 9, 11 and 13 in Figure 1. The box-girder is supported on single-column concrete bents and abutments that are monolithic with it. The columns are octagonal in shape and 8 × 5.5 ft (2.4 × 1.7 m) in size. Their height ranges from 24 to 76 ft (7.3–23.2 m).

The bridge was designed by the California Department of Transportation (Caltrans) in 1969 and the construction was completed in 1973. During 1991–1992 the bridge was retrofitted by Caltrans under a program to increase seismic safety of bridges with single-column bents. This was accomplished by improving the ductility of concrete columns, strengthening the existing foundations, and by upgrading the connections between the adjacent bridge segments. To improve ductility, 0.375 in (0.95 cm) thick steel jackets

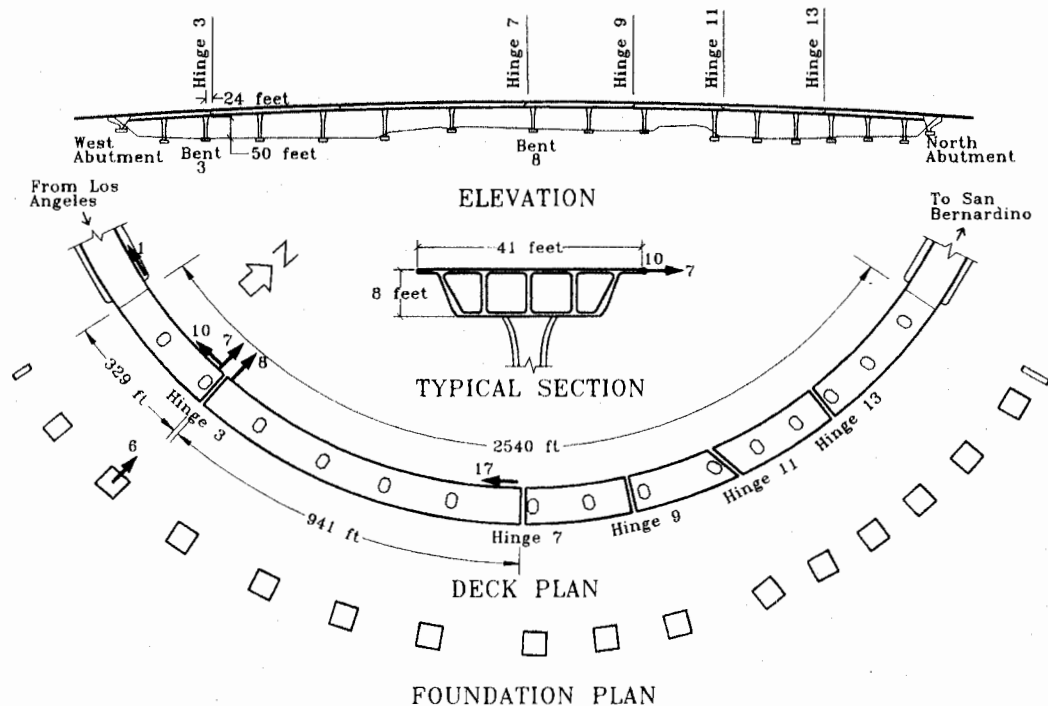


Figure 1. Plan and elevation of the Caltrans I-10/215 interchange bridge in San Bernardino, California showing locations of selected seismic sensors. Only six (1, 6, 7, 8, 10 and 17) of the total 34 sensors are shown here. Arrows indicate the positive direction of motion measured by the sensors (1 ft = 0.3048 m)

were installed around existing columns, and the gaps between the jackets and the columns filled with grout. The foundations were strengthened by increasing their size. Supplemental support for the box-girder was provided at each abutment. The connections at the hinges were improved by tying together adjacent segments of the box-girder with new cable restrainers that replaced those already in place. A typical cable restrainer unit, shown in Figure 2, consists of twenty 0.75 in (1.9 cm) diameter cables, between 16 and 21 ft (4.9 and 6.4 m) long.

Strong-motion instrumentation and earthquake records

Seismic instrumentation of the bridge by CSMIP was completed in early 1992. A total of 34 strong-motion sensors (accelerometers) were installed to measure the motions of selected points at (1) the base of concrete columns; (2) the abutments; and (3) the bridge deck. Of particular interest in this instrumentation was the response of the bridge at the hinges. Sensors were installed at each of the five hinges to measure the transverse motions of the adjacent bridge segments. At some hinges the longitudinal and vertical motions are also measured. Selected sensors are shown by numbered arrows in Figure 1, where the arrows indicate the positive direction of motion measured by the sensors. Sensor 6, for example, measures the transverse motion at the base of Bent 3, and Sensor 1 measures the longitudinal motion of west abutment. The positive direction of motion for Sensors 6, 7 and 8 is in the radially inward direction. The positive motion for Sensors 1, 10 and 17 is tangential to the bridge in the clockwise direction. The complete instrumentation scheme and recorded data are discussed in detail by Huang and Shakal.¹

The unprocessed acceleration records for the Landers and Big Bear earthquakes from all 34 sensors on the bridge were included in two CSMIP data reports.^{2,3} The processed records from these two earthquakes (in the form of accelerations, velocities, displacements, and response-spectra) were published subsequently by CSMIP.⁴ The records obtained from sensors near the hinges were of special significance

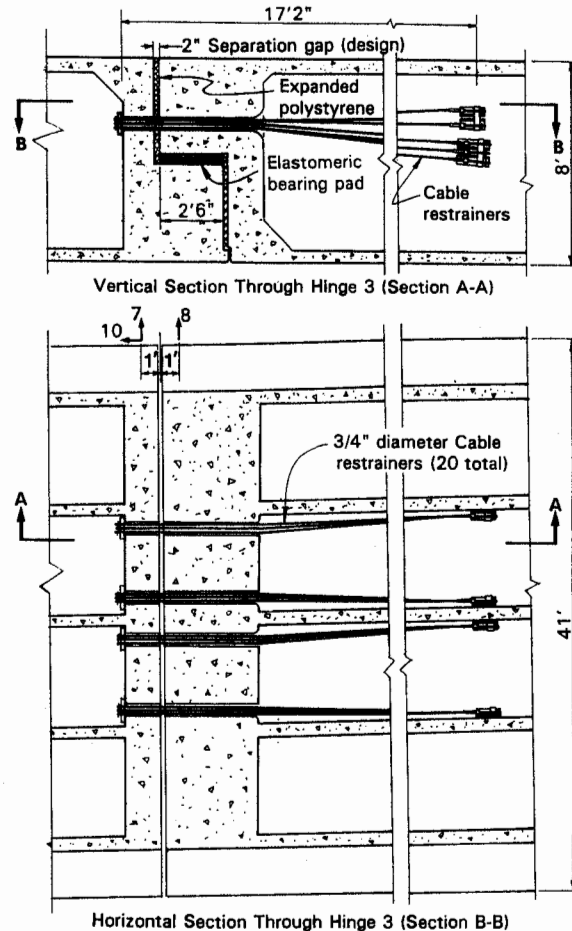


Figure 2. Horizontal and vertical sections at Hinge 3 showing the separation gap, cable restrainers, and elastomeric bearing pad (from Caltrans construction drawings). Numbered arrows indicate the sensor locations and the direction of measured motions (not drawn to scale) (1 in = 0.0254 m)

because of intermittent sharp spikes, as high as $1.0g$. The peak ground accelerations, however, were only about $0.1g$.

Scope and objectives

The objectives of this paper are to: (1) Identify the mechanism(s) responsible for the observed spikes, and (2) estimate the magnitude of the forces involved. For this purpose records obtained during the Landers earthquake from Sensors 1, 6, 7, 8, 10 and 17 are studied in detail. These records are shown in Figure 3.

SEISMIC INTERACTION AT A HINGE

Hinge 3 on the bridge (see Figure 1) is selected for a detailed investigation of the interaction between adjacent segments of the box-girder. A vertical section through Hinge 3, in Figure 2, shows that the right segment is supported by the left segment and rests on an elastomeric bearing pad. There is a horizontal separation between the two segments, provided to accommodate temperature-induced expansion. The separation gap had a width of 2 in (5 cm) at the time of construction; its actual width at the time of the earthquakes might have been different depending upon the effect of aging on concrete and actual temperature at the time of

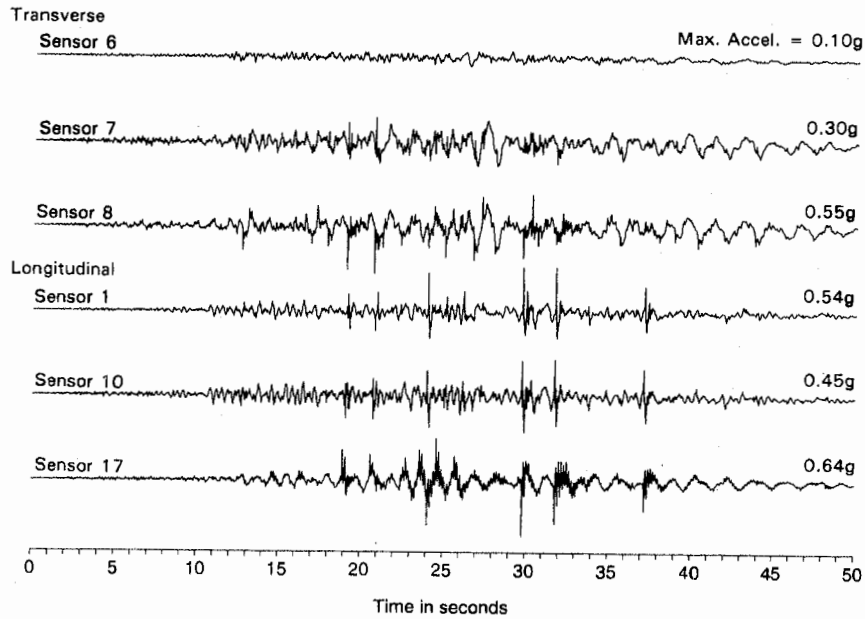


Figure 3. Acceleration records of Sensors 1, 6, 7, 8, 10 and 17 (Figure 1) obtained during the 28 June 1992 Landers earthquake in Southern California

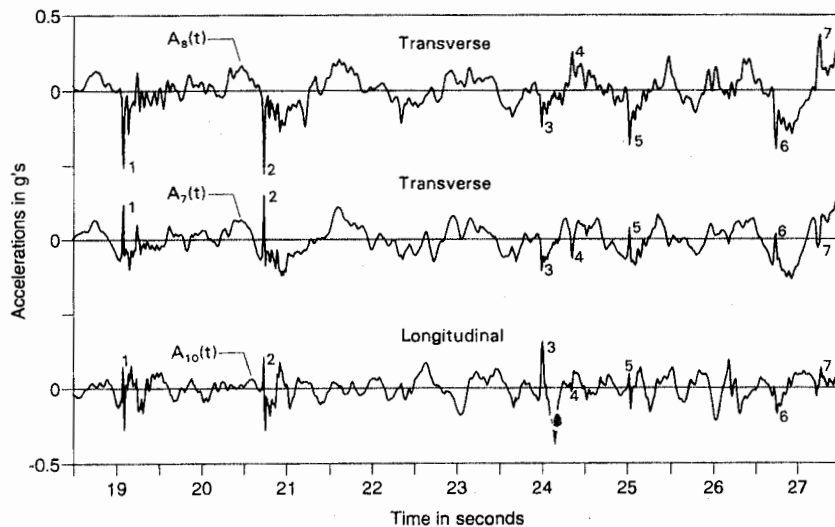


Figure 4. Acceleration records at Hinge 3 from 18.5 to 27.5 s into the record, showing simultaneous occurrence of spikes in the transverse, $A_7(t)$ and $A_8(t)$, and longitudinal, $A_{10}(t)$, directions

earthquakes. According to Caltrans design drawings, the cable restrainers were given an initial slack to allow approximately 2 in (5 cm) relative movement between the bridge segments during temperature variations. Two concrete shear keys (not shown in Figure 2) were provided at each hinge to prevent excessive relative movement in the transverse direction.

At Hinge 3 the transverse motions of the left and the right segments of the box-girder are measured by Sensors 7 and 8, respectively. In addition, the longitudinal motion of the left segment is measured by Sensor 10. The acceleration records of these three sensors, in Figure 3, contain a series of intermittent sharp spikes.

The spikes are more clearly visible in the shorter, 9 s, segments of these records that are shown in Figure 4. Note the following:

- (i) The spikes appear in sets, occurring simultaneously in each of the three records in Figure 4; seven sets of spikes appeared during the 18.5–27.5 s interval.
- (ii) With the exception of Spike 3, the transverse spikes (in the records of Sensors 7 and 8) are equal in magnitude and opposite in direction to each other; the third spike in these two records points in the same direction.

Spikes of similar nature can be observed in the published records from all hinges of the bridge during both the Landers and Big Bear earthquakes.^{2–4}

Due to the absence of spikes in the base input motion, measured by Sensor 6 (see Figure 3), it is apparent that the observed spikes are not directly caused by the ground input motion. Whereas, the response without the spikes is a direct result of the amplification of ground motion through the height of the bridge, the spikes are caused by interaction between the adjacent bridge segments at the hinges. Three different mechanisms that would produce the observed spikes are discussed below.

Interaction mechanisms

The equal and opposite transverse spikes (Spikes 1, 2, 4, 5, 6 and 7 in Figure 4) suggest the presence of equal and opposite transverse forces generated at Hinge 3. Two mechanisms (Mechanisms 1 and 2) that will give rise to these forces are as follows:

Mechanism 1-frictional contact. In this mechanism, illustrated in Figure 5(a), the two adjacent segments of the box-girder, undergoing predominantly transverse motion, come in contact with each other. Upon contact

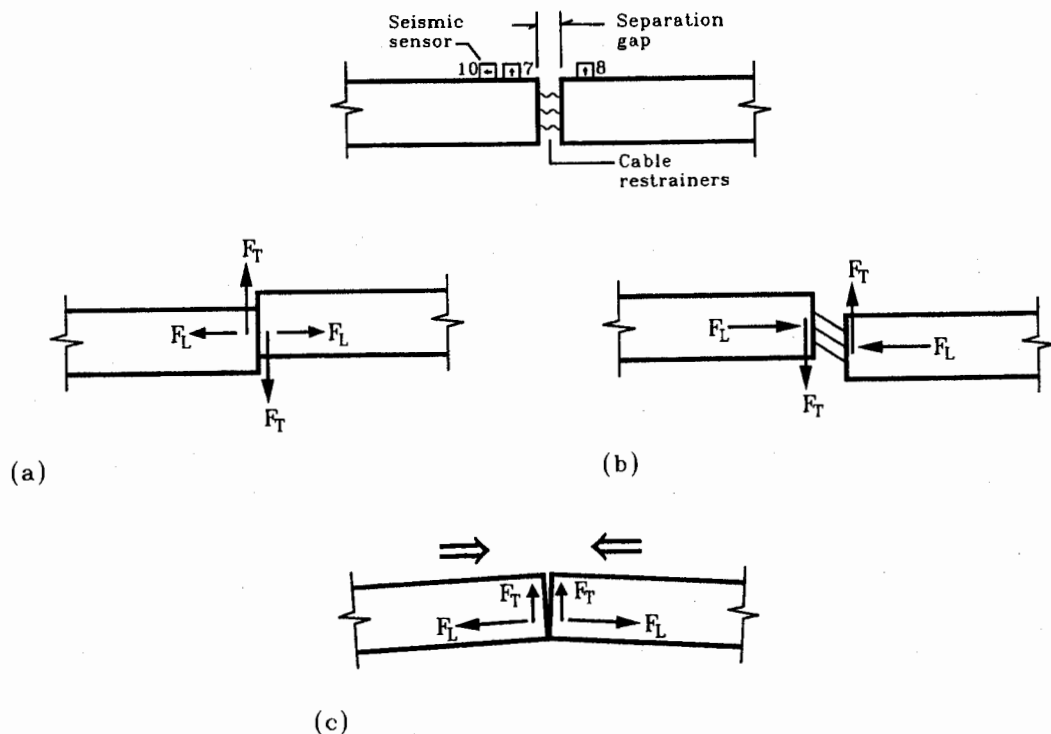


Figure 5. Plan views at Hinge 3 illustrating: (a) Mechanism 1-frictional contact between adjacent segments undergoing predominantly transverse motion; (b) Mechanism 2-cable engagement between adjacent segments undergoing predominantly transverse motion; and (c) Mechanism 3-head-on impact between adjacent segments undergoing predominantly longitudinal motion. F_T = transverse force, F_L = longitudinal force; solid arrows indicate the direction of forces generated

a pair of equal and opposite frictional forces, F_T , are generated in the transverse direction. These forces are in turn responsible for the observed equal and opposite spikes in the transverse direction. Note that an axial compressive force is also generated in this mechanism. This force is responsible for the longitudinal spike.

Mechanism 2-cable restraint. In this mechanism, illustrated in Figure 5(b), the two adjacent segments, undergoing predominantly transverse motion, move far enough away from one another that the cable restrainers between them become engaged and generate forces that pull the two segments back toward each other. In this case the component of the cable forces in the transverse direction, F_T , is responsible for the spikes in that direction. The axial tensile force, F_L , which is equal in magnitude to the longitudinal component of the cable force, is responsible for the spike in the longitudinal response measured by Sensor 10.

It could be argued that the transverse spikes in the records were caused by the engagement of shear keys rather than by frictional and cable forces generated in Mechanisms 1 and 2. The engagement of shear keys alone, however, cannot explain the simultaneous occurrence of spikes in the longitudinal direction, because the shear keys were designed to allow free longitudinal movement.

After analysing the longitudinal spikes in the next section it is deduced that Spikes 1, 2, 5 and 6 were caused by Mechanism 1 (frictional contact), and Spikes 4 and 7 were caused by Mechanism 2 (cable restraint). The third set of spikes in Figure 4 cannot be explained by either Mechanism 1 or 2 because the transverse spikes in this set are not equal and opposite to each other. A clue to the mechanism that would give rise to the third set of spikes is provided by the large longitudinal response corresponding to this set of spikes (see $A_{10}(t)$ in Figure 4). This mechanism is as follows.

Mechanism 3-head-on impact. Spikes in this mechanism are generated by a head-on impact between adjacent bridge segments undergoing predominantly longitudinal motion. The response in this case is, therefore, primarily longitudinal, although a certain amount of transverse response is also generated. One possible cause of the transverse response is illustrated in Figure 5(c) in which the two adjacent segments are shown to impact against each other at a slight angle. Upon impact a pair of transverse forces, F_T , pointing in the same transverse direction, is generated which is responsible for nearly identical transverse spikes.

FORCES OF INTERACTION

As noted above, the spikes in the record of Sensor 10 in Figure 4 were caused by the longitudinal forces of interaction generated by Mechanisms 1-3. Upon closer examination of the longitudinal spikes in Figure 4 it is seen that each of these spikes consists of a pair of peaks in the opposite directions. These spikes are more appropriately referred to as 'doublets'. Note that for Doublets 1, 2, 3, 5 and 6 a positive peak is followed by a negative peak, while for Doublets 4 and 7 it is vice versa—a negative peak followed by a positive peak. The sign reversal of the doublet peaks is more clearly visible in Figure 6 where the lower two plots of Figure 4 are redrawn at an expanded horizontal scale in the vicinity of Doublets 2 and 7. The shape of Doublet 2 in the record of Sensor 10 may be approximated by a single cycle of a sinusoidal function, i.e.

$$A(t) = A_{\max} \sin\left(\frac{2\pi t}{\tau}\right) \quad (1)$$

where τ is the duration of the doublet, and A_{\max} is its amplitude. As previously mentioned, Doublet 2 was caused by an axial force generated by Mechanism 1 or 2. Whether the axial force is compressive or tensile will determine if the doublet was caused by Mechanism 1 or by Mechanism 2. In the following discussion a simple model is used to determine the shape and size of the axial force pulse that produced Doublet 2.

Model

The segment of the box-girder to the left of Hinge 3 is represented by a semi-infinite rod of uniform cross-section area \bar{A} as shown in Figure 7(a). Assume an unknown axial force $F(t)$ is suddenly applied at the

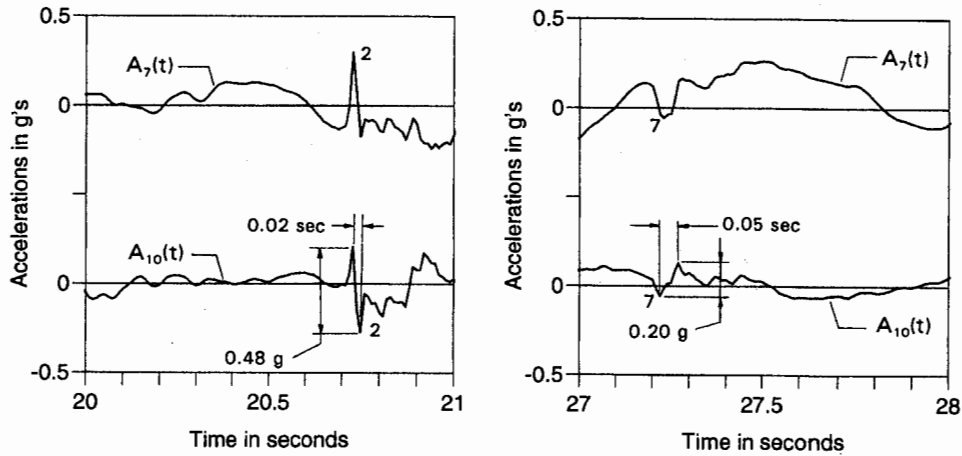


Figure 6. Acceleration records in the vicinity of Spikes 2 and 7 in Figure 4 in the transverse, $A_7(t)$, and longitudinal, $A_{10}(t)$, directions

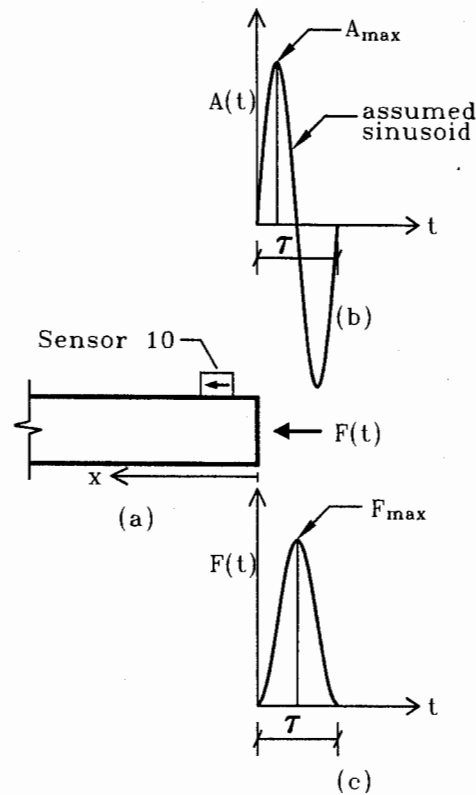


Figure 7 (a) Plan view of the box-girder model used to study the relationship between (b) a hypothetical acceleration spike $A(t)$ similar to those measured by Sensor 10, and (c) the axial force pulse $F(t)$ that would be generated at the end of the box-girder model

right end of this rod, and that this force produces an acceleration response at that end of the rod of the form given by equation (1) and shown in Figure 7(b). The objective is to determine the force $F(t)$ from this acceleration response. Initially, assume that the applied force is compressive. A negative sign at the end of the analysis would then imply a tensile force.

The applied force $F(t)$ give rise to a compressive stress wave that travels to the left with the compressive wave velocity c , given by⁵

$$c = \sqrt{\frac{Eg}{w}} \quad (2)$$

where E is the Young's modulus of elasticity, w the weight density and g the acceleration due to gravity.

A displacement function of a wave propagating with velocity c in the positive x -direction has the form⁵

$$u(x, t) = f(x - ct) \quad (3)$$

where $u(x, t)$ is the displacement at time t of a point at distance x from the right end, and f is some unknown function. The acceleration $A(x, t)$ can then be obtained by double differentiation of the displacement $u(x, t)$ with respect to time t ,

$$A(x, t) = \frac{\partial^2 u(x, t)}{\partial t^2} = c^2 f''(x - ct) \quad (4)$$

where the prime denotes derivative with respect to $(x - ct)$. The compressive stress $\sigma(x, t)$ is obtained by multiplying the axial compressive strain, $-\partial u/\partial x$, by the Young's modulus of elasticity E ,

$$\sigma(x, t) = -E \frac{\partial u(x, t)}{\partial x} = -E f'(x - ct) \quad (5)$$

Using equations (4) and (5), the following relationship is established between the derivative of compressive stress and the acceleration:

$$\sigma'(x, t) = -w \frac{A(x, t)}{g} \quad (6)$$

The compressive stress is then obtained from the measured acceleration by performing the integral

$$\sigma(x, t) = -w \int_0^{x-ct} \frac{A(x, t)}{g} d(x - ct) \quad (7)$$

The expression for a forward propagating acceleration wave $A(x, t)$ is obtained by simply replacing t by $t - x/c$ in equation (1), which amounts to stating that the response at $x = 0$ is repeated at an arbitrary value of x after a time lapse of x/c . The resulting expression is

$$A(x, t) = -A_{\max} \sin(x - ct) \frac{2\pi}{c\tau} \quad (8)$$

Substituting equation (8) into equation (7) and performing the integral yields the following expression for the forward propagating compressive stress wave:


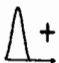

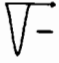


$$\sigma(x, t) = \frac{A_{\max}}{g} \frac{c\tau w}{\pi} \left[\frac{1}{2} \left(1 - \cos(x - ct) \frac{2\pi}{c\tau} \right) \right] \quad (9)$$

The force $F(t)$ can then be obtained by multiplying $\sigma(0, t)$ by the cross-section area \bar{A} , i.e.

$$F(t) = \frac{A_{\max}}{g} \frac{c\tau w}{\pi} \left[\frac{1}{2} \left(1 - \cos \frac{2\pi t}{\tau} \right) \right] \times \bar{A} \quad (10)$$

The force $F(t)$ is plotted in Figure 7(c), below the assumed acceleration form shown in Figure 7(b). During time τ the force builds up from zero to a maximum value and then drops to zero again. Its positive sign implies that the force is compressive. Since the assumed acceleration form (Figure 7(b)) was chosen to approximate the shape of Doublet 2 in Figure 4, the doublet was, therefore, produced by a compressive force generated during contact between the adjacent segments in Mechanism 1.

Table I. Identification of spike-causing mechanisms in records of Sensors 7, 8 and 10 shown in Figure 4

Mechanism	Transverse spikes in records of Sensors 7&8	Shape of longitudinal doublet in record of Sensor 10	Shape of axial force pulse*	Spike no.
1	Equal & opposite			1, 2, 5 & 6
2	Equal & opposite			4 & 7
3	Equal & same polarity			3

* + = compressive; - = tensile.

The results of the above analysis are summarized in the top row of Table I which essentially states that Mechanism 1 produces equal and opposite spikes in the transverse direction and a sinusoidal doublet in the longitudinal direction. Spikes 1, 2, 5 and 6 in Figure 4 were, therefore, caused by Mechanism 1. Rows two and three of Table I are generated by simple deduction. It is stated in the second row that Mechanism 2, like Mechanism 1, produces equal and opposite spikes in the transverse direction but a reverse sinusoidal doublet in the longitudinal direction (caused by an axial tensile force). Spikes 4 and 7 were, therefore, caused by Mechanism 2. The third row of Table I indicates that Mechanism 3 produces transverse spikes that are nearly equal to each other, and a longitudinal doublet that has a sinusoidal shape similar to Mechanism 1. Spike 3, therefore, corresponds to Mechanism 3.

Forces of impact

Substituting the term in the square brackets in equation (10) by its maximum value of unity, the expression for the maximum value of the axial force F_{\max} is obtained as follows:

$$F_{\max} = \frac{A_{\max}}{g} \frac{c\tau w}{\pi} \times \bar{A} \quad (11)$$

By making use of equation (11) one can compute the forces generated at Hinge 3 from the size (amplitude and duration) of the longitudinal doublets. For Doublet 2 (Figure 6), $A_{\max} = 0.24g$, and $\tau = 0.04$ s. From the recorded data, the compression wave velocity c is later estimated to be 11 000 ft/s (3300 m/s). The weight density of concrete $w = 145$ lb/ft³ (22.8 kN/m³). The cross-section area of the box-girder, estimated from construction drawings, is $\bar{A} = 10\,000$ in² (6.45 m²). Upon substituting these values in equation (11) one obtains $F_{\max} = 338$ kips (1500 kN). Assuming that the entire cross-section of the box-girder comes in contact when the two segments collide, the maximum compressive stress is $\sigma_{\max} = F_{\max}/\bar{A} = 34$ psi (230 kPa).

The largest doublet in the record of Sensor 10 is Doublet 3 (see Figure 4). Its large size is not unexpected because it is associated with Mechanism 3 in which a head-on impact occurs between adjacent bridge segments. Although the shape of Doublet 3 is not strictly sinusoidal a rough estimate of the force responsible for this doublet can still be obtained by the use of the simple formula given by equation (11). This force is nearly ten times (≈ 3000 kips [13.34 MN]) the force that caused Doublet 2, and the corresponding stress is $\sigma_{\max} = 300$ psi (2.07 MPa). During the 20–40 s interval in the record of Sensor 10 four doublets of similar shape and size occurred at 24.01, 29.76, 31.75 and 37.15 s (see Figure 3). Each of these is believed to have been

caused by head-on impact between adjacent segments at Hinge 3. It will be seen later that the effect of these impacts was felt even at locations away from Hinge 3.

Forces in cable restrainers

As previously noted, Doublet 7 in Figure 6 was caused by sudden engagement of the cable restrainers between adjacent segments. Equation (11) can also be used to estimate the tensile force in the box-girder (force F_L in Figure 5(b)) caused by cable restraint. For Doublet 7, $A_{\max} = -0.10g$ and $\tau = 0.10$ s. Upon substituting these into equation (11), one obtains a net maximum tensile force in the box-girder of 350 kips (1570 kN). Assuming that the tensile force in the box-girder is not significantly different from the net force in the cables (the former is actually a longitudinal component of the latter), one obtains an average tensile force in each of the 20 cables of $350/20 = 17.5$ kips (78.5 kN). The actual force in some cables may be higher since not all the cables are necessarily engaged at the same time. The stress in a 0.75 in (1.9 cm) diameter cable corresponding to a tensile force of 17.5 kips is 39.6 ksi (273 MPa).

Comparison between actual and allowable stresses

According to the design drawings, structure concrete with 28 day compressive strength $f'_c = 3250$ psi (22.4 MPa) was used for the box-girder segment to the left of Hinge 3. For the segment to the right of Hinge 3, cast-in-place prestressed concrete with $f'_c = 4300$ psi (29.6 MPa) was used. At the time of Landers earthquake, nearly 20 years after construction, it is reasonable to assume that f'_c had approached a value of more than 5 ksi (34.5 MPa).⁶ According to Caltrans design specifications,⁷ the allowable compressive stress in concrete is $0.4f'_c = 2000$ psi (13.8 MPa), and the modulus of rupture is $7.5\sqrt{f'_c} = 530$ psi (3.65 MPa). The splitting tensile strength, which is between 50 and 70 per cent of the modulus of rupture,⁸ is about 325 psi (2.24 MPa).

The maximum value of the compressive stress pulse generated by impacts in Mechanism 3 is estimated to be approximately 300 psi (2.07 MPa). This value is only 15 per cent of the allowable value. A compressive pulse is, however, reflected as a tensile pulse, of equal amplitude, from the free end of the medium in which it travels.⁵ In other words, a compressive pulse generated at Hinge 3 is reflected as a tensile pulse from Hinge 7. A tensile stress of 300 psi is nearly as high as the splitting tensile strength of concrete.

As noted above the maximum stress induced in the cable restrainers is estimated to be 39.6 ksi (273 MPa). This value is 23% of the yield stress $F_y = 176$ ksi (1220 MPa).⁹

SOME IMPORTANT OBSERVATIONS

Propagation of compression wave

Because the velocity with which a compression wave travels through concrete is finite, a small amount of time must elapse before the effect of a force generated at one location is felt at another location. An evidence of wave propagation from Hinge 3 to other locations on the bridge is presented here with reference to the records of Sensors 1, 10 and 17 in Figure 3. Sensor 10 is located at Hinge 3; Sensor 1 is located at the west abutment, 329 ft (100 m) to the left of Hinge 3; and Sensor 17 is located at Hinge 7 which is 941 ft (287 m) to the right of Hinge 3.

As mentioned earlier, four large spikes, caused by head-on impacts between adjacent segments at Hinge 3 were detected by Sensor 10 at 24.01, 29.76, 31.75 and 37.15 s. Each of these spikes is followed by a similar looking spike in the record of Sensor 1 (see Figure 3). The digital data revealed that the spikes in the record of Sensor 1 occurred 0.03 s after those in the record of Sensor 10. The time lapse between spikes is more clearly visible in Figure 8 in which the records from Sensors 1, 10 and 17 are shown for a 29–32 s interval. Since the spikes detected by Sensor 1 could not have originated at the west abutment, which is monolithic with the box-girder, it is evident that these spikes actually travelled leftward, from Hinge 3 to the west abutment. Upon dividing the distance between west abutment and Hinge 3 by the travel time of 0.03 s, one obtains the velocity of propagation of compression wave to be 11 000 ft/s (3300 m/s).

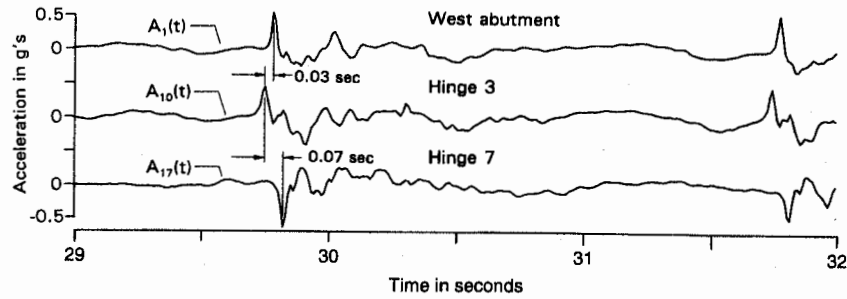


Figure 8. Acceleration records of Sensors 1, 10 and 17 illustrating propagation of compression wave from Hinge 3 (A_{10}) to the west abutment (A_1) and to Hinge 7 (A_{17})

The spikes generated at Hinge 3 also travelled to Hinge 7, which is 941 ft (287 m) to the right of Hinge 3. Upon examining the records of Sensors 10 and 17 in Figures 3 and 8 it is observed that each of the large spikes detected by Sensor 10 is followed by another spike detected by Sensor 17. Note also that the spikes detected by Sensor 17 are opposite in direction to those detected by Sensor 10. This is expected since Sensors 10 and 17 are located on opposite sides of Hinge 3 where the spikes were generated. From the digital data the travel time to Sensor 17 was obtained as 0.07 s. Upon dividing the distance between Hinges 3 and 7 by the travel time, one obtains the velocity of propagating compression wave to be 13 400 ft/s (4100 m/s). This value is nearly 20 per cent higher than the value for the leftward propagation of the compression wave (from Hinge 3 to the west abutment). This difference is reasonable considering that there is an uncertainty of 0.005 s in the values of the travel time, and a higher grade of concrete was used for the right prestressed concrete segment.

Estimation of concrete compressive strength f'_c from strong-motion data

Observed values of wave propagation velocity c may be used to back calculate f'_c by first computing the Young's modulus of elasticity E using equation (2) and then obtaining f'_c from the empirical relation^{7,8}

$$E = 57\,000\sqrt{f'_c} \quad (12)$$

in which both E and f'_c are in psi. The value of f'_c computed in this manner is 4.4 ksi (30.3 MPa) for the structure concrete segment and 9.7 ksi (66.9 MPa) for the prestressed concrete segment. However, it should be noted that f'_c can only be approximately estimated in this manner (an error of 0.005 s in the travel time will result in a 7–8 per cent error in wave propagation velocity c which in turn will result in 30–40 per cent error in the estimated value of f'_c).

Periodic motion triggered by impacts

An examination of the record of Sensor 17 in Figure 3 reveals the presence of two distinct frequencies in the response measured by this sensor. Of these, the lower-frequency response (with approximate period of 1.2 s) corresponds to the fundamental period of the bridge structure (box-girder-column frames) in the longitudinal direction. Upon closer examination it is observed that the higher-frequency response is most prominent after each large spike. It was therefore triggered by impacts at Hinge 3 and is the response of the box-girder segment, between Hinges 3 and 7, undergoing axial deformations. The periodicity of this response is more clearly visible in Figure 9 in which a 2 s interval (31–33 s) in the record of Sensor 17 is shown; note that the response period is 0.15 s.

If the segment between Hinges 3 and 7 were assumed to be a straight, prismatic, free-ended rod of length L , its fundamental period of axial vibration T would be given by⁵

$$T = \frac{2L}{c} \quad (13)$$

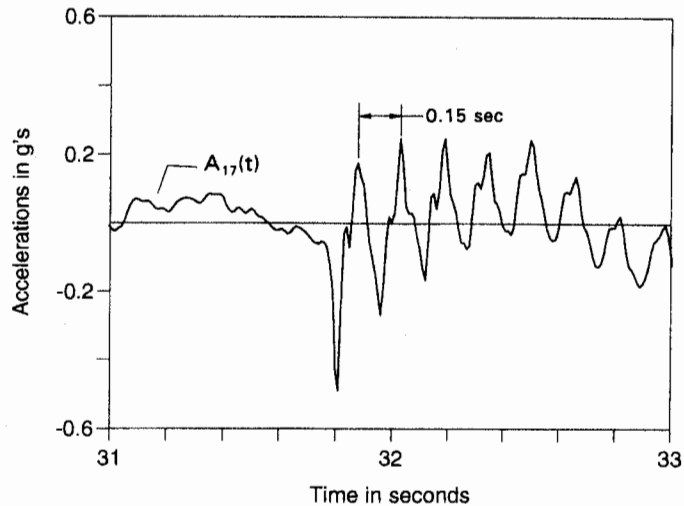


Figure 9. Acceleration record of Sensor 17 illustrating periodic response of the box-girder segment between Hinges 3 and 7, triggered by impact at Hinge 3

Upon substituting $L = 941$ ft (286.8 m) and $c = 13\,400$ ft/s (4.08 km/s) into equation (13), one obtains $T = 0.14$ s which is within 7 per cent of the observed value of the period, thus establishing that the higher frequency response was indeed triggered by impacts at the hinge.

CONCLUSIONS

This paper is focused on the interpretation and analysis of sharp spikes in the acceleration records obtained during a recent California earthquake from an instrumented concrete bridge. The principal conclusions are as follows.

1. The spikes were caused by forces generated at the separation joints (hinges) by the interaction between adjacent segments of the box-girder. The interaction occurred both by impacts and by engagement of the cable restrainers that tie together adjacent segments of the box-girder.
2. The forces of impact and cable restraint can be estimated from the amplitude and duration of the acceleration spikes using a simple formula. Results obtained from the strong-motion records indicate that reasonably high forces were generated at the hinges during the 1992 Landers earthquake. However, the resulting stresses estimated were below the yield values for the cable restrainers and concrete.
3. In some instances the spikes recorded at a particular location did not actually originate at that location. They travelled from their source to other locations on the bridge with the velocity of a compression wave propagating through concrete. The longitudinal spikes recorded at the west abutment, for example, actually originated at Hinge 3 where impacts between adjacent segments of the box-girder occurred.

ACKNOWLEDGEMENTS

The California Strong Motion Instrumentation Program (CSMIP) worked closely with the California Department of Transportation (Caltrans) in the installation of seismic strong-motion equipment on the I10/215 interchange bridge. The encouragement of J. Gates of the Division of Structures and the cooperation of the staff at the Caltrans District 8 office are appreciated. CSMIP also extends its appreciation to members of the Strong Motion Instrumentation Advisory Committee and its Lifelines Subcommittee. The sensor layout for the bridge was developed by J. Ragsdale, C. Ventura, M. Huang and A. Shakal. It was reviewed by

B. Douglas (University of Nevada-Reno), J. Gates (Caltrans), R. Imbsen and D. Liu (Imbsen & Associates), P. Jennings (Caltech), J. Penzien (U.C. Berkeley), J. Raggett (J.D. Raggett & Associates), S. Werner (Dames & Moore), and J. Wilson (McMaster University). Their reviews and comments on the sensor locations improved the instrumentation scheme for the bridge.

The records obtained at the bridge were made possible through the efforts of many CSMIP technicians who installed and maintained the equipment at the bridge. C. Petersen and R. Payne coordinated the extensive effort of installation and record recovery.

The comments of two anonymous reviewers are appreciated.

REFERENCES

1. M. Huang and A. Shakal, 'CSMIP strong-motion instrumentation and records from the I-10/215 interchange in San Bernardino', *Earthquake spectra*, 11(2), (1995).
2. A. Shakal, M. Huang, T. Cao, R. Sherburne, R. Sydnor, P. Fung, P. Malhotra, C. Cramer, F. Su, R. Darragh and J. Wampole, 'CSMIP Strong-Motion Records From the Landers, California Earthquake of 28 June 1992', *Report OSMS 92-09*, California Department of Conservation, Division of Mines and Geology, Office of Strong Motion Studies, August 1992.
3. M. Huang, A. Shakal, T. Cao, R. Sherburne, R. Sydnor, P. Fung, P. Malhotra, C. Cramer, F. Su, R. Darragh and J. Wampole, 'CSMIP Strong-Motion Records From the Big Bear, California Earthquake of 28 June 1992', *Report OSMS 92-10*, California Department of Conservation, Division of Mines and Geology, Office of Strong Motion Studies, August 1992.
4. R. Darragh, T. Cao, M. Huang and A. Shakal, 'Processed CSMIP Strong-Motion Records From the Landers and Big Bear, California Earthquakes of 28 June 1992: San Bernardino-I10/215 Interchange', *Report OSMS 93-08*, California Department of Conservation, Division of Mines and Geology, Office of Strong Motion Studies, September 1993.
5. R.W. Clough and J. Penzien, *Dynamics of Structures*, 2nd edn, McGraw-Hill, New York, 1993.
6. Caltrans, 'Interim memo to designers (20-4)', California Department of Transportation, April 1992.
7. Caltrans, 'Bridge design specifications (9-7)', California Department of Transportation, June 1990.
8. R. Park and T. Paulay, *Reinforced Concrete Structures*, J. Wiley, New York, 1975.
9. Caltrans, 'Bridge design aids (14-16)', California Department of Transportation, December 1991.

